ARTICLE

Check for updates

Self-organized patterning on azo molecular glass film via optical near-field effect

Zenan Wang[1], Hao Huang [1] & Xiaogong Wang [1✉]

Self-organized surface patterning has attracted great research interest ranging from scientific understanding to various applications. Here, we report a unique patterning behavior observed on an azo molecular glass film with polystyrene microspheres on the surface upon irradiation with a circularly polarized laser beam. Photoinduced submicron hillocks are found to organize into concentric arrays around isolated polystyrene spheres, while more complex patterns are observed around two or more spheres close to each other. The irradiation first creates surface relief rings encircling the spheres and then the rings split into hillocks arranged in circular arrays with increasing exposure time. Pattern formation is shown to be controlled by synergy from the optical near-field of polystyrene spheres with the spontaneous hillock formation characteristics of the molecular glass film upon light irradiation. This work is beneficial to deepening the understanding of light–matter interactions and is expected to be applied in different areas.

[1] Department of Chemical Engineering, Laboratory of Advanced Materials (MOE), Tsinghua University, Beijing 100084, PR China.
✉email: wxg-dce@mail.tsinghua.edu.cn

The formation of complex submicron patterns on surfaces has attracted great research interest ranging from scientific understanding to diverse applications[1–6]. Various surface patterns have been fabricated from different materials and widely applied in microelectronics, optics, photonics, flexible optoelectronics, and bio-mimicking architectures[7–11]. In recent years, azo polymers and azo molecular glasses (polymers and molecular amorphous materials containing azo chromophores) have emerged as a fascinating class of new material used for surface patterning through light irradiation[12–21]. Distinct from conventional photolithography via photochemical reaction of a photoresist, the pattern formation on azo polymer and azo molecular glass films is achieved by mass transfer induced by radiation and thus-formed patterns are erasable and reconfigurable[12,13]. A well-documented case is the formation of surface-relief-gratings (SRGs) on azo polymer films[22,23], and azo molecular glass films[16], upon irradiation with interfering laser beams. More complex surface patterns have been created by multiple interfering fringe superposition[12,19], optical near-field of metal nanostructures[24–26], and vortex-beam illumination[27]. Furthermore, simply by irradiation with a single laser beam, spontaneous surface patterns are formed on films of azo polymers and azo molecular glasses, which are generally classified into self-organized surface patterns[28–32]. One typical type of spontaneously formed structure appears as hillock arrays with local hexagonal order induced by circularly polarized light (CPL) irradiation. The heights of hillocks are around 100 nm depending on the exposure energy, while the distances between hillocks are in submicron scale related to the light wavelength[29–32]. Similar to SRGs, the spontaneously formed patterns are stable below the glass transition temperature (T_g) of the material and erasable upon raising the temperature to above T_g. Azo molecular glasses differ from azo polymers by their much lower molecular weights[33–37]. Without the entanglements of polymer chains, azo molecular glasses usually show a high efficiency to form SRGs and other surface structures upon light irradiation[16,36,37]. The formation of spontaneous surface patterns on azo molecular glass films is promising for surface patterning via single-step irradiation with a continuous wave low-intensity laser[30,31]. However, at the current stage, producing complex surface patterns in a controllable manner by this method and understanding its mechanism are still facing great challenges.

In recent years, near-field nanolithography upon the interaction of colloidal spheres with light for surface patterning has attracted more and more attention[38–40]. The transparent spherical particles represent a unique class of microscale optical elements with a series of interesting effects related to the optical near-field. Distinct from the optical enhancement of metallic nanomaterials owing to surface plasmonic resonance, the near-field effect of dielectric particles is mainly related to light scattering from the objects[38,39]. The light scattering by spherical particles is well described by Mie theory with the size parameter $q = 2\pi Rn/\lambda$, depending on the wavelength (λ), refractive index (n), and radius (R) of microspheres[41]. For particle sizes close to the wavelength ($q \sim 2\pi$), the surface spheres illuminated by plane wave generate an annular scattering profile with high intensity on the contacted substrate area[42,43]. Increasing the sphere size further ($q > 2\pi$), the focusing effect is enhanced near the sphere surface of the shadowed side, known as photonic nanojet[38,44–46]. The optical near field produced by colloidal spheres has been intensively studied over the past years for various applications. Upon the optical near field produced by a pulse laser, nano-holes and their arrays have been inscribed on the surfaces of different materials, such as silicon wafer[47], glass surface[48], polyimide foil[49], Al surface[50], and others[39,40]. In these cases, films beneath the microspheres are ablated by concentrated electromagnetic waves due to the local field enhancement. With optically trapped microspheres, the near field effect has been

applied to write various subwavelength patterns directly[51]. Using a photoresist, three-dimensional (3D) nanolithography via light scattering from colloidal particles has been accomplished to produce structures such as hollow 3D and hollow-core nanostructures[52,53]. With a photosensitive crystalline $Ge_2Sb_2Te_5$ film with deposited spheres on the surface, the scattering light intensity distribution has been recorded as a two-dimensional pattern obtained by crystalline-to-amorphous transition upon pulse laser irradiation[54]. More closely related to the current study, topographical nanostructure patterning has been performed upon the optical near field of polystyrene microspheres on thin films of azo polymers, such as azobenzene-containing urethane-urea copolymer and polyurethane[55,56]. Indented surfaces with high resolution are formed in this way, where the depth and diameter of the dents depend on the sizes of the polystyrene spheres. The dent formation is attributed to the mass migration induced by the near-field gradient force beneath the spheres[57–59]. Although both spontaneous formation of hillocks on azo material surface and patterning upon optical near field effects have been investigated, to our knowledge, no study on the synergy of these two powerful patterning methods has been reported in the literature yet.

In this study, we found a very interesting phenomenon related to the optical near-field effect of polystyrene microspheres and self-organized patterning behavior of an azo molecular glass (IA-Chol). The spontaneously formed hillocks on IA-Chol films well organize into concentric arrays with local hexagonal order and other types of patterns around the microspheres upon the irradiation with CPL. To understand this intriguing phenomenon, three types of polystyrene spheres with diameters (D) of 250, 500, and 1000 nm were selected and their effects on the pattern formation were investigated by the irradiation with CPL from a continuous wave laser at two wavelengths ($\lambda = 488$ nm and 532 nm). Other important factors affecting self-organized pattern formation were also experimentally investigated. As revealed by the observations, the hillock arrangements around the spheres are regulated by the optical near field of polystyrene spheres, while the local structure parameters are determined by the self-organized patterning behavior of IA-Chol. The mechanism of the pattern formation is elucidated on the basis of the experiments and finite element method (FEM) calculation.

Results and discussion

Self-organized pattern formation. Figure 1 shows the material, experimental scheme, and some representative observations of this study. IA-Chol is an organic compound consisting of isosorbide core, two *push-pull* type azo chromophores, and peripheral cholesteryl groups (Fig. 1a). Its synthesis and characterization have been given in our previous report[60], also shown in the Supplementary Information (Supplementary Methods, for NMR and MS spectra see Supplementary Figs. 1–10). IA-Chol exhibits a strong absorption band in the visible light range with λ_{max} of 441 nm (Supplementary Fig. 11). The *push-pull* type azo chromophores are known to undergo rapid *trans-cis-trans* isomerization cycles under visible light irradiation to cause mass migration[12,13,19]. Thin films with polystyrene microspheres on the smooth surfaces were obtained by a procedure described in "Methods" section. The optical and SEM micrographs of the microspheres on substrates are shown in Supplementary Fig. 12. For light irradiation, the laser beam propagates along the negative Z-axis of the Cartesian coordinates and impinges the film at the X–Y plane (Fig. 1b). Since there is no difference for irradiations with right circularly polarized (RCP) light and left circularly polarized light (Supplementary Fig. 13), RCP light used in this study is referred to as CPL without further distinction. Figure 1c, d gives SEM images of IA-Chol film with polystyrene spheres on the surfaces before and after CPL irradiation. The concentric arrays of hillocks around the isolated polystyrene spheres are formed after the irradiation. In
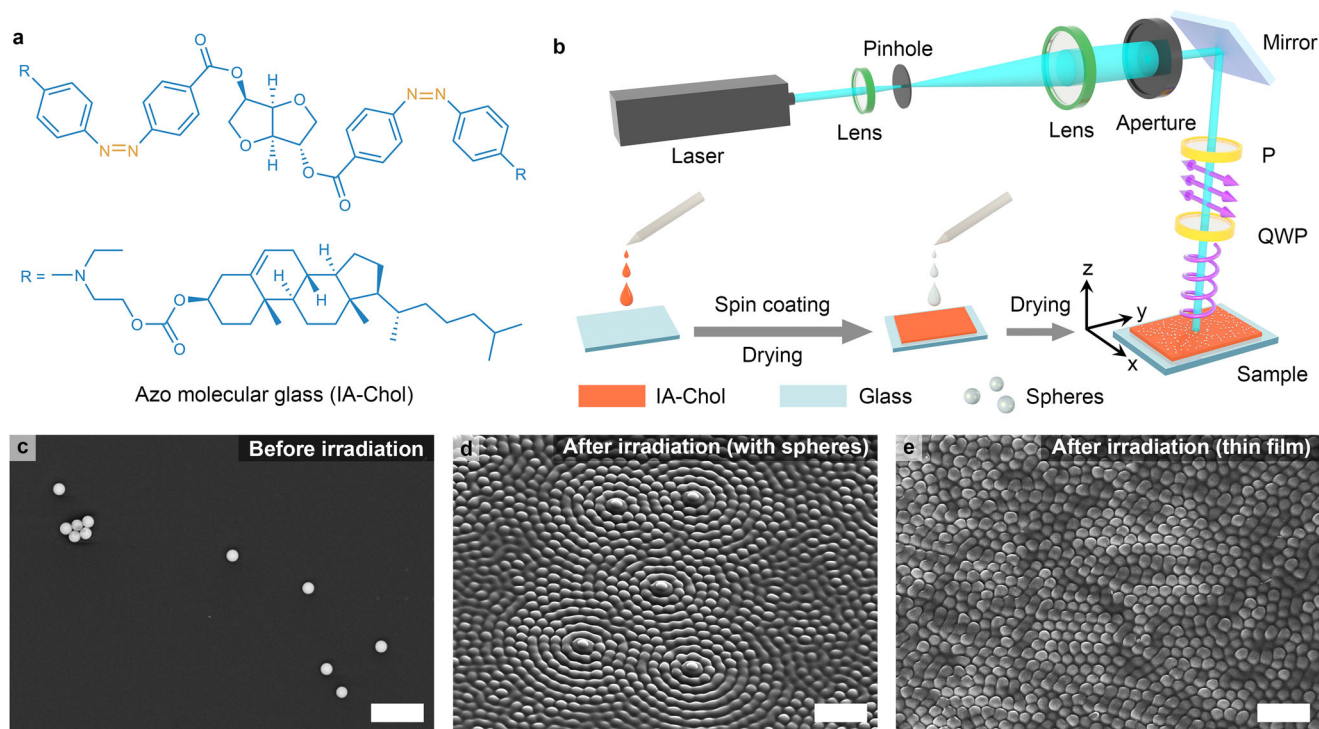
Fig. 1 Molecular structure, experimental setup and surface pattern formation on IA-Chol film surface via optical near-field effect of polystyrene spheres. a The chemical structure of IA-Chol. **b** Schematic of sample preparation and the optical setup used to create the circularly polarized laser beam. **c** The SEM (top-view) image of the IA-Chol film with polystyrene spheres ($D = 500$ nm) on the surface before the irradiation. **d** The SEM (side-view) image of the IA-Chol film with polystyrene spheres ($D = 500$ nm) on the surface after irradiation with the circularly polarized light for 30 min. **e** The SEM (top-view) image of the IA-Chol thin film without the polystyrene sphere on the surface after irradiation with the circularly polarized light for 60 min. The light intensity and wavelength were 300 mW cm^{-2} and 488 nm. The scale bars in the microscopic images correspond to 2 μm.

contrast, without the polystyrene spheres, the hillocks formed on the IA-Chol film via CPL irradiation only show local hexagonal order (Fig. 1e).

Figure 2 gives magnified SEM images of IA-Chol films with the polystyrene spheres ($D = 500$ nm) on the surfaces after exposed to CPL for 30 and 60 min. After CPL irradiation for 30 min, the hillocks are arranged in several concentric circles around isolated spheres over a range of several microns (Fig. 2a, b). The inset in Fig. 2a gives the E-field norm ($|\mathbf{E}|$) distribution on IA-Chol film around the sphere, calculated by FEM (COMSOL Multiphysics, see details in Methods part). The concentric rings of $|\mathbf{E}|$ distribution with alternate intensity variation result from the interference of the incident light with that scattered from the sphere. As presented below in "Mechanism and optical simulation", the concentric arrangement of the hillocks is controlled by the $|\mathbf{E}|$ distribution. A close inspection shows that more complicated patterns appear when two or more spheres are close to each other, which also correspond to the interference fields of scattered and incident lights around the spheres. The observation reveals a unique function of the scattered light from polystyrene microspheres to control the arrangement of self-organized structures. The round rims attached on polystyrene spheres are also observed, which are caused by mass transfer away from the regions beneath the spheres due to the focused laser beam[55,56]. After the irradiation for 60 min, the main surface characteristics remain unchanged, but the rims start to merge with the closest hillocks (Fig. 2c). The self-organized pattern formation is affected by irradiation time, sphere size, light wavelength, and polarization as presented below in details.

Structure evolution with irradiation time. Figure 3 shows the surface morphology transition of the IA-Chol films with the

polystyrene spheres ($D = 500$ nm) after being exposed to CPL for different time periods. With the irradiation time increase, the encircling structures around polystyrene spheres change gradually. The evolution of concentric structures around isolated spheres can be clearly identified to show the following characteristics. After being exposed to CPL for 10 min, the concentric rings are formed on the IA-Chol film surfaces around polystyrene spheres (Fig. 3a, b, Supplementary Fig. 14a, b). For the irradiation of 20 min, the concentric rings show a tendency to split into separate hillocks, and the rims attached to the spheres are observed (Fig. 3c, d, Supplementary Fig. 14c, d). When irradiated for 30 min, the rings almost completely split into separate hillocks (Fig. 2a, b, Fig. 3e, f, Supplementary Fig. 14e, f). Further increasing the exposure time to 60 min, the heights of hillocks increase and the rims merge with the nearby hillocks, but no obvious variation of the concentric arrangement is observed (Fig. 2c, Supplementary Figs. 14g, h, 15a, b). Similar variations with the irradiation time are observed on regions around two and more spheres, though the patterns become more complicated due to the interference fields. It is worth noting that as the heights of the newly formed structures are much smaller than the sizes of polystyrene spheres ($D = 500$ nm and $D = 1000$ nm as well), a small detection range is required in the AFM analysis to facilitate the observation of surface morphology. Therefore, the heights of polystyrene spheres in atomic force microscope (AFM) images are out of the detection range and not properly indicated by the height bars. Supplementary Fig. 16a–d compare the AFM images with different detection ranges, which show that only the heights of the newly formed structures are correctly represented by the AFM height bars with the small detection range. The vertical distances of polystyrene spheres above surface need to be measured separately with a large detection range.
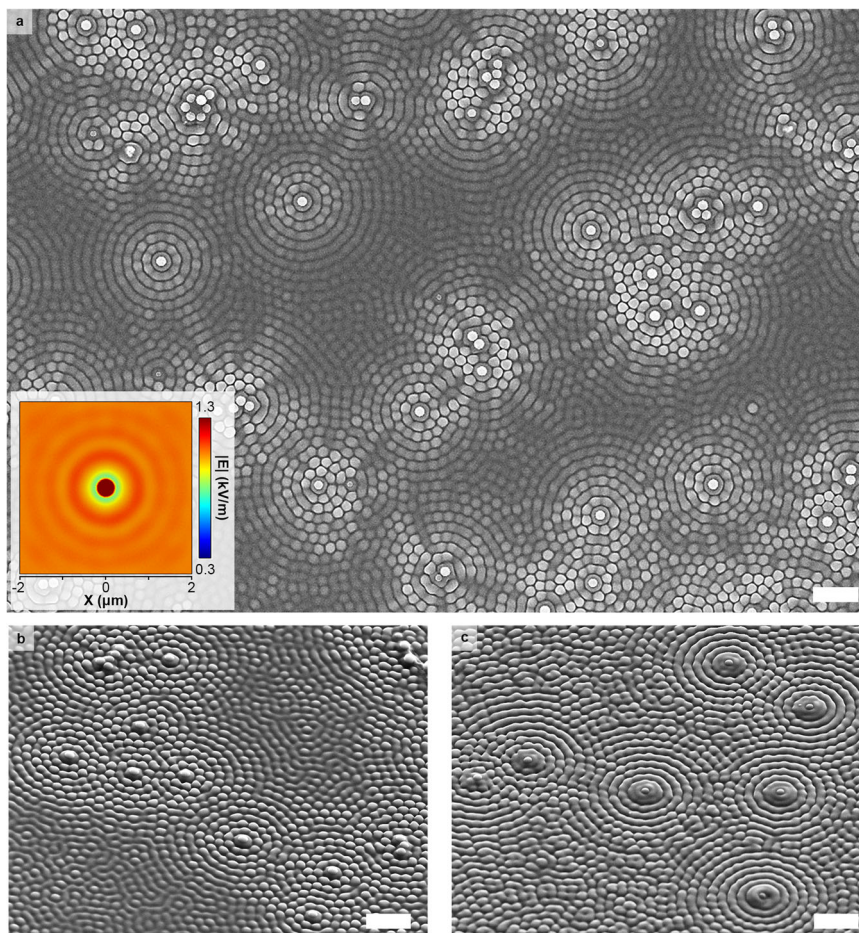
Fig. 2 Typical top-view and side-view SEM images of the IA-Chol films with polystyrene spheres ($D = 500$ nm) on the surfaces after being exposed to the circularly polarized light for different time periods. a Top-view, irradiation for 30 min. The inset shows the E-field norm distribution on the surface of the IA-Chol film with the polystyrene sphere ($D = 500$ nm) exposed to the circularly polarized light ($\lambda = 488$ nm), which was simulated by COMSOL Multiphysics. **b** Side-view, irradiation for 30 min. **c** Side-view, irradiation for 60 min. The light intensity and wavelength were 300 mW cm^{-2} and 488 nm. The scale bars of all the SEM images correspond to 2 μm.

The structure formation and evolution are closely related to the scattered light from the polystyrene spheres. Without polystyrene spheres on IA-Chol film surface, only random relief stripes appear after irradiation for 20 min, which split into hillocks after irradiation for 30 min (Supplementary Fig. 17a, b). Even after CPL irradiation for 60 and 120 min, only hillocks with the local hexagonal order are observed on the surface (Fig. 4a, Supplementary Fig. 17c). In contrast, for the film with the surface spheres (Fig. 4b), the hillocks organize into the concentric arrays in regions influenced by the scattered light from the spheres (Region 1). Meanwhile, the hillocks only show local order in regions not obviously affected by the scattered light (Region 2). The influences of the interference fields around several spheres are uncovered by the more complicated patterns on the surfaces (Supplementary Figs. 18 and 19). The growth rates of hillocks in Region 1 and 2 with the irradiation time are obviously different, and the latter is similar to that of IA-Chol film without the spheres on the surface (Fig. 4c). For CPL irradiation of 20 min, the average height of hillocks in Region 1 is 45 ± 5 nm, while the height of hillocks in Region 2 is only 17 ± 3 nm, similar to that of the film without polystyrene spheres on the surface (17 ± 5 nm). When irradiated with CPL for 30 min, the average height of hillocks in Region 1 increases to 99 ± 7 nm, and those for the other two cases are 48 ± 6 and 47 ± 9 nm, respectively. After being exposed to CPL for 60 min, the average heights of

the hillocks in Region 2 and on the film without polystyrene spheres become almost the same as the average height of those in Region 1, all of which no longer show increase with further irradiation. Although the heights all undergo a gradual increase with the irradiation time, the hillocks in Region 1 grow faster compared with the other two cases within the first 30 min. This is attributed to the fact that the formation of the hillocks in Region 1 is through the ring-to-hillock transition, so they are obviously higher than those in Region 2 in this time period. The structure parameters of the hillocks obtained by AFM are summarized in Supplementary Table 1. Although the self-organized pattern in Region 1 is distinctively different from those in Region 2 and on film without the polystyrene spheres, the distances between the adjacent hillocks are almost the same for these three cases. After irradiation for more than 30 min, some irregularity appears in the final patterns for thin films both devoid of or deposited with polystyrene spheres, which is related to the surface expansion due to the repeated *trans-cis* isomerization for a long time[61,62].

The average radii of the concentric structures around isolated spheres are important parameters characterizing the self-organized patterns. Supplementary Figure 20a illustrates the four innermost circles around a sphere, where the first circle is the rim attached on the sphere. The averaged radii of rims and circular arrays obtained from SEM images are plotted versus the
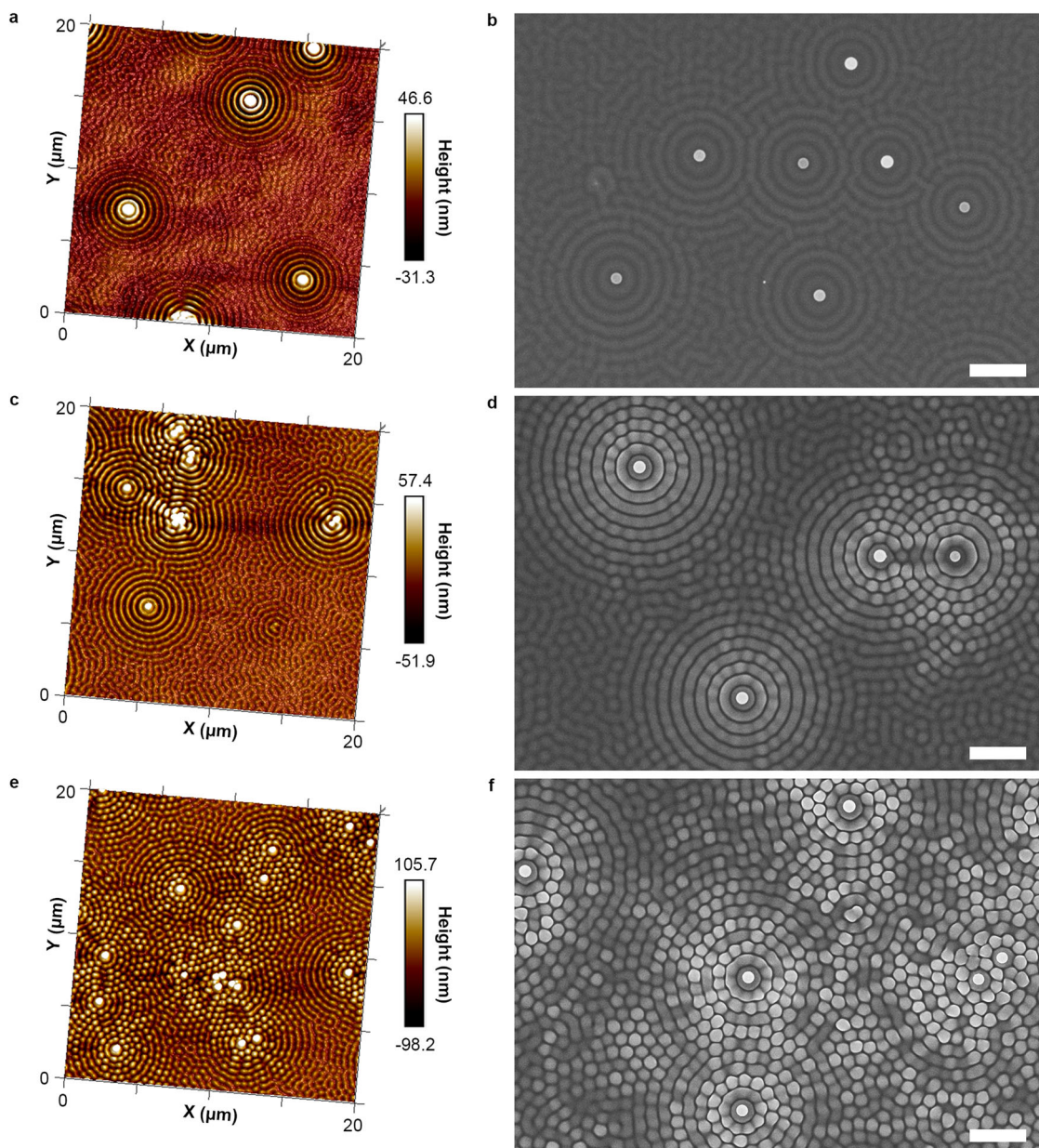
Fig. 3 Typical AFM images and top-view SEM images of the IA-Chol films with polystyrene spheres ($D = 500$ nm) on the surfaces after exposure to the circularly polarized light for different time periods. a, b 10 min; **c, d** 20 min; and **e, f** 30 min, respectively. **a, c, e** AFM images; and **b,d, f** top-view SEM images. The light intensity and wavelength were 300 mW cm^{-2} and 488 nm. The scale bars of all the SEM images correspond to 2 μm.

irradiation time (Supplementary Fig. 20b). Distinct from the annular hillock rings, the rims are generated by the mass transfer away from the areas beneath the spheres. The light-focusing effect of a polystyrene sphere is verified by the E-field norm ($|\mathbf{E}|$) distribution calculated by FEM (COMSOL Multiphysics). The model and calculation result are given in Supplementary Figure 21a, b, while those of the IA-Chol film without polystyrene sphere on the surface are given in Supplementary Figure 22a, b for comparison. The dents beneath the spheres and their rims are formed through the mass transfer in the direction from the high light intensity to low intensity in the light-focused zone[57–59]. Due to their different formation pathways, the rims become observable in the period from 10 min to 20 min, while the radii of other circular arrays show the increase in this period accompanied by ring-to-hillock transition. Further increasing the irradiation time to 30 min, the radii of the rims and circular hillock arrays only show a small increase.

Figure 5 gives AFM images of IA-Chol films with polystyrene spheres ($D = 500$ nm) on the surfaces after irradiation with a low intensity (150 mW cm^{-2}) CPL for different time periods. The structures formed on the surfaces with the irradiation time of 20, 40, 60, and 120 min are almost the same as those obtained after irradiation with the intensity of 300 mW cm^{-2} for 10, 20, 30, and 60 min discussed above. This result indicates that the structure formation is determined by the exposure energy (intensity × time), which is consistent with those of the spontaneous structure formation on film for this type of material[61,62]. Moreover, the self-organized structure formation is a reversible process (Supplementary Fig. 23). By raising the temperature to 170 °C, the photo-induced annular hillock structures on the IA-Chol film were erased, though the dents beneath the polystyrene spheres could not revert back to the original plane. By dispersing polystyrene spheres on the thus-recovered film and irradiating with CPL through the same procedure again, the hillocks were
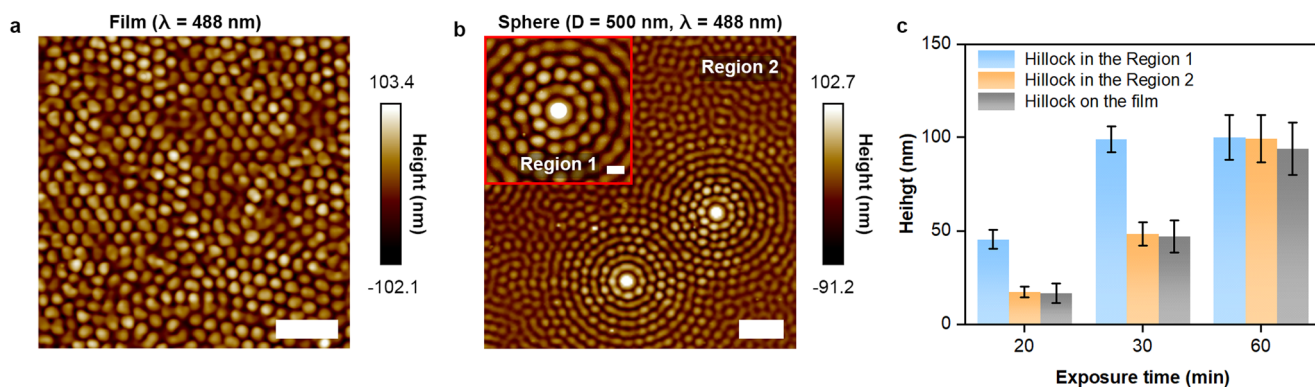
Fig. 4 Comparison of the irradiation results of the IA-Chol thin films without and with polystyrene spheres (D = 500 nm) on the surfaces. a Typical AFM image of IA-Chol film exposed to the circularly polarized light for 60 min. **b** Typical AFM image of IA-Chol film with polystyrene spheres (D = 500 nm) on the surface exposed to the circularly polarized light for 30 min, where the inset shows the magnified image of Region 1. **c** The heights of hillocks in Region 1, Region 2 and on the thin film without the spheres versus the irradiation time. The light intensity and wavelength were 300 mW cm^{-2} and 488 nm. The scale bars of AFM images in **a** and **b** correspond to 2 μm, while the scale bar in the inset of **b** corresponds to 500 nm. The error bars in **c** represent the standard deviation, where each data point is obtained from five independent samples.
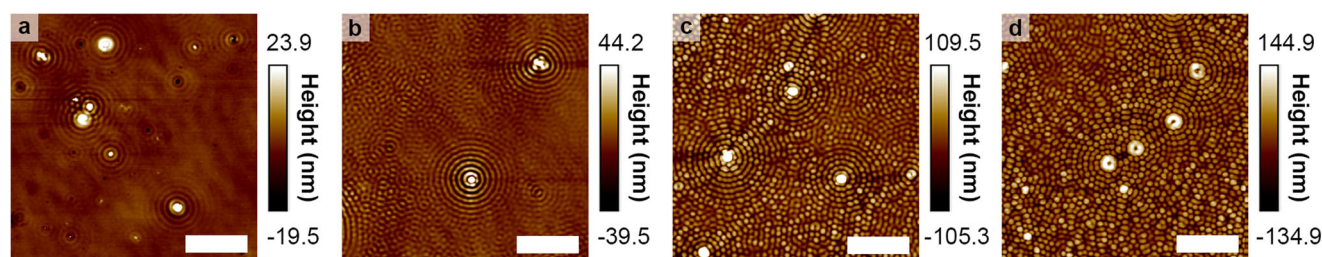

Fig. 5 Two-dimensional AFM images of the IA-Chol film with polystyrene spheres (D = 500 nm) on the surfaces after being exposed to the circularly polarized light (λ = 488 nm) for different time periods. a 20 min, **b** 40 min, **c** 60 min, **d** 120 min. The scale bars of all the AFM images correspond to 5 μm. The light intensity and wavelength were 150 mW cm^{-2} and 488 nm.

observed to form concentric rings around the polystyrene spheres on the IA-Chol film surface. These observations indicate that the self-organized structure formation is neither a photo-ablation process nor directly related to the thermal effect.

Influences of microsphere sizes. The size of microsphere is a very important factor to influence pattern formation. Sphere size can significantly affect the light-focusing behavior as described by the size parameter (q)[38,40]. With the q increase, the field profile tends to be more localized in the forward direction and the field intensity is significantly enhanced[38,47,50]. Moreover, the interaction between a sphere and surface also increases with the sphere size. For the interaction of the sphere with the surface through van der Waals forces, the net interaction energy is proportional to D/h, where h is the distance of the sphere away from the surface[63,64]. As h is much smaller than D, the sphere-surface interaction is generally strong enough to keep spheres on the surface and this attraction force increases with the particle size. To understand the influences of sphere sizes on self-organized pattern formation, polystyrene spheres with D = 250 and 1000 nm were adopted to carry out the investigation in comparison with 500 nm spheres discussed above. Although their light scattering behavior is still described by Mie theory, the microspheres with D = 250 and 1000 nm can also be considered as a scatterer in line with Debye theory and focusing micro-lens, respectively[38–41].

The morphologies of the IA-Chol films with polystyrene spheres (D = 250 nm) on the surfaces after CPL (488 nm) irradiation are shown in Fig. 6a-c and Supplementary Fig. 24a–d. The relief rings are formed around the spheres after irradiation

for 2 and 3 min, but disappear for irradiation of 5 min. This is attributed to the relatively quick immersion of the spheres in IA-Chol films as revealed by cross-section profiles of AFM. Supplementary Figure 25 shows a typical case, where the polystyrene sphere starts to sink into the film around 2 min and is almost complete buried under surface within 5 min. The immersion in IA-Chol film is caused by the mass migration away from the dents below the spheres. The quicker immersion compared with the case of 500 nm sphere is caused by the spread of the |**E**| profile in the shadowed side of the sphere. This can be seen by comparing the FEM simulation results for the spheres with diameters of 250, 500, and 1000 nm (Supplementary Figs. 21b, 26a–d). For the case of 250 nm sphere, the mass transfer of IA-Chol produces a dent with a larger size than the sphere to cause quicker immersion. Extending the exposure time to 10 min, only holes in the original positions with the spheres can be seen on the IA-Chol film (Supplementary Fig. 27a). Due to the quick immersion, the interfering wave from the scattered light only causes the shallow relief structures (Fig. 6a, b), and the structures are erased during the further irradiation (Fig. 6c). After the light irradiation for 20 min, the formed surface structures are similar to those found on the IA-Chol film without spheres (Supplementary Fig. 27b). This random hillock pattern remains unchanged with increasing exposure time to 60 min (Supplementary Fig. 27c).

The optical near-field effect of polystyrene spheres with D = 1000 nm on the surfaces is quite different as revealed by the investigation through the same procedure. After CPL irradiation for 10 min, the concentric relief rings are observed around the spheres (Fig. 6d, Supplementary Fig. 28a, b, Supplementary Fig. 29a). Continuing irradiation to 20-30 min,
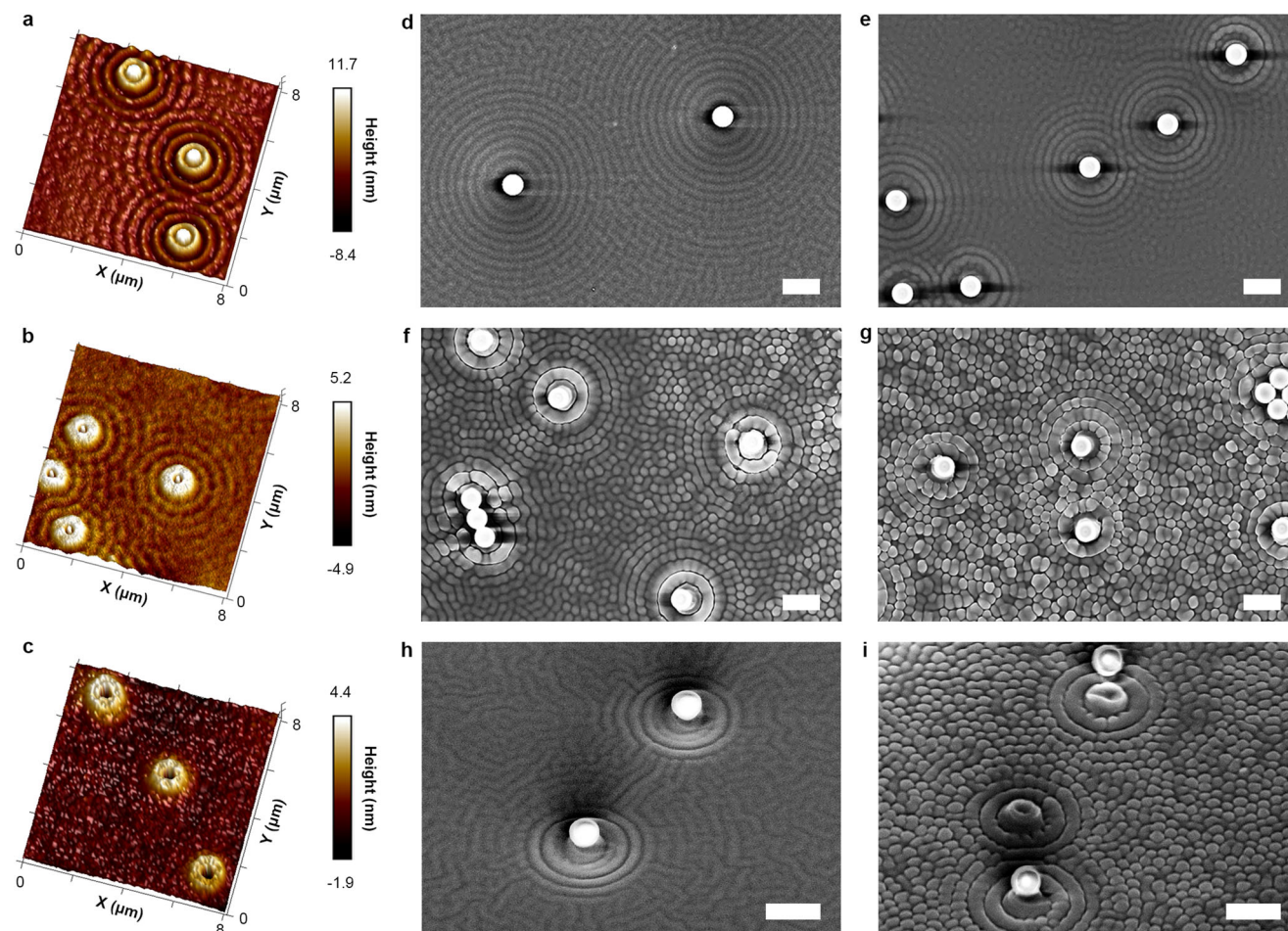
Fig. 6 The microscopic images of the IA-Chol films with the polystyrene spheres (D = 250 nm, 1000 nm) on the surfaces after irradiation with the circularly polarized light for different time periods. a–c Typical three-dimensional AFM images of IA-Chol films with polystyrene spheres (D = 250 nm) on the surfaces exposed to the light for 2, 3 and 5 min, respectively. **d–g** Top-view SEM images of IA-Chol films with polystyrene spheres (D = 1000 nm) on the surfaces exposed to the light for 10, 20, 30, and 60 min, respectively. **h, i** Side-view SEM images of IA-Chol films with polystyrene spheres (D = 1000 nm) on the surfaces exposed to the light for 20 min and 30 min. The light intensity and wavelength were 300 mW cm^{-2} and 488 nm. The scale bars of all the SEM images correspond to 2 μm.

the concentric rings split into hillocks arranged in circular arrays around the spheres (Fig. 6e, f, Supplementary Figs. 28c–f, 29b, c). Further increasing illumination time to 60 min, the hillocks can still be clearly seen, while their circular arrangements become less ordered (Fig. 6g, Supplementary Figs. 28g, h, 29d). Distinct from the cases of the polystyrene spheres with D = 250 nm and 500 nm, the humps are formed beneath the spheres when irradiated with CPL for 20–30 min (Fig. 6h, i, Supplementary Fig. 30). The shapes of the humps under the spheres can be clearly seen when some spheres fall off from the humps (Fig. 6i, Supplementary Figs. 29e–g, 30). The hump formation for 1000 nm spheres is attributed to the significantly enhanced light-focusing effect on the shadowed side. As shown by the FEM simulation (Supplementary Fig. 26d), the light is highly convergent in the area beneath the 1000 nm sphere. In the initial period, the dents with diameters obviously smaller than the sphere sizes are formed under spheres, caused by the mass transfer from the higher |**E**| areas to lower |**E**| areas. Increasing irradiation time, the humps are formed beneath the spheres when the overall exposure energy of the focused beam exceeds a threshold value, causing the dents and rims to protrude from the surface.

The above results show that a suitable sphere size is critically important to produce well-organized surface patterns. For the

500 nm spheres, the relief structures with high enough amplitudes form in the first 10 min (the first stage), so that the well-organized hillock arrays are obtained through ring-to-hillock transition in the second stage. In contrast, well-organized structures can hardly be formed by using spheres with small and large sizes. Due to the quick immersion of 250 nm spheres, the relief structures formed in the first 2–3 min have shallow grooves and are almost completely erased at 5 min. Therefore, the structures formed in the first 2–3 min have little influence on hillock arrangement emerging in the second stage, which only shows the local hexagonal order (Supplementary Fig. 31a). On the other hand, for the 1000 nm spheres, the hillocks organize into circular arrays after the irradiation for 30 min (Supplementary Fig. 31b). However, because the spheres start to rise above the surface around 10 min, the interference field formed by the scattered light from spheres and incident light gradually changes positions with the irradiation time. Therefore, the patterns become less order with increasing irradiation time to 60 min. Moreover, the 1000 nm spheres are easy to fall off from the humps and displaced during the irradiation process. Due to the weak influence of the 250 nm spheres, the hillocks only with the local order have a smaller average height compared with those around 500 nm and 1000 nm spheres after CPL irradiation for 30 min (Supplementary Fig. 31c). On the other hand, the distances

between the centers of the adjacent hillocks reflecting the local organization are all around 488 nm by using the three types of polystyrene spheres (Supplementary Fig. 31d).

Correlation with light wavelength and polarization. To understand the influences of the wavelength, the pattern formation on IA-Chol films with 500 nm polystyrene spheres on the surfaces was investigated by irradiation with 532 nm CPL. The irradiation with 532 nm light is also a typical way to induce the self-organized structures on azo soft matter films[31,32,61]. Similarly, the encircling relief structures around the spheres are formed in the first 10 min and then split into the hillocks in circular arrays (Supplementary Fig. 32a–h). The structure parameters of the self-organized patterns obtained after light irradiation for 30 and 60 min are given in Supplementary Table 2. An obvious difference from the case using 488 nm light is that the spontaneously formed hillocks in Region 2 and on the film without the polystyrene spheres show heights almost equal to those in Region 1 after the irradiation for 30 min. Comparing the results in Supplementary Table 1 shows that the hillocks in Region 2 and on the film without the polystyrene spheres obviously grow faster for 532 nm light irradiation. Therefore, the hillock heights do not show obvious differences for those in Region 1, 2, and on surface without the spheres after the irradiation with 532 nm CPL for 30 min. This more efficient way to form self-organized surface structures and SRGs by 532 nm irradiation has been observed on azo molecular glasses and azo polymers bearing similar azo chromophores[31,65,66]. When the excitation wavelength is located between λ_{max} and the absorption band tail at the longer wavelength side, the radiation shows a higher surface modulation ability compared with light with a shorter wavelength. This observation is attributed to the $n-\pi^*$ transition band buried in the strong absorption band of $\pi-\pi^*$ transition at this wavelength so that the light irradiation can more efficiently trigger *trans-cis-trans* isomerization cycles and cause mass transfer as well[13,19,65]. Moreover, the diameters of the hillocks show obviously larger values for those obtained by 532 nm CPL irradiation, especially for those in Region 1. The distances between adjacent hillocks are almost equal to the light wavelength (532 nm), which are the same with or without the spheres on the surfaces (Supplementary Fig. 33). The radii of the concentric hillock arrays obtained from the microscopic images show larger values compared with those upon the 488 nm irradiation (Supplementary Table 3). It is caused by the increased spatial period of the interference field due to the longer wavelength. The partial immersion behavior of 500 nm spheres in IA-Chol films upon irradiation shows some differences for these two wavelengths (Supplementary Fig. 34a, b). The polystyrene spheres gradually sink in the IA-Chol films in the first 20 min of the irradiation, which manifests a faster and deeper immersion for 488 nm light irradiation (Supplementary Fig. 35a). The displaced volume of the material beneath the spheres also shows a more significant increase for 488 nm light irradiation in this period (Supplementary Fig. 35b). The influences of the partial immersion of polystyrene spheres and other dynamic factors will be discussed below.

The light polarization state also shows a critically important influence on pattern formation. As shown by SEM (Supplementary Fig. 36a), the patterns induced by linearly polarized light (LPL) with a wavelength of 488 nm are completely different from those discussed above. For the irradiation of 5 min, both relief rings surrounding spheres and relief bands in outside regions are observed (Supplementary Fig. 36b). When the irradiation time increases to 10 min, the ripples perpendicular to the electric vibration direction of LPL prevail in most regions

(Supplementary Fig. 36c). Further increasing the irradiation time to 20–30 min, the ripple structures almost occupy the whole surface area leaving only circular distortions around the spheres (Supplementary Fig. 36d, e). The ripple formation is typical responsive behavior of azo polymer and azo molecular glass films upon LPL irradiation[28–32]. The encircling structures formed in the first stage are incompatible with the ripples formed in the second stage and are taken over by the latter in the pattern formation process.

Mechanism and optical simulation. The formation of hillocks with local hexagonal order has been observed on azo polymer and azo molecular glass films upon laser irradiation[28–32]. The discovery of the current study is that the spontaneously formed hillocks can well organize into encircling arrays around polystyrene spheres. The above observations show that the pattern formation includes two stages, i.e., forming the encircling relief structures around the spheres, and splitting the structures into hillocks with self-organized arrangements. The formation of the encircling relief structures around the spheres is caused by the interference fields around the spheres. The |**E**| distributions obtained by COMSOL Multiphysics are given in Supplementary Fig. 37a–f, including CPL of 488 nm and 532 nm and the spheres with the three diameters. The concentric |**E**| distributions around the spheres are the same for all these cases. To more clearly unfold the correlation, the calculated |**E**| distribution is compared with a typical AFM image of IA-Chol film surface around a polystyrene sphere after the light irradiation at 488 nm for 10 min (Fig. 7a, b). In order to see the morphology beneath the sphere, the film with the polystyrene spheres was placed vertically on the optical bench during the irradiation to let some spheres to fall off from the surface (Supplementary Fig. 38a, b), which is distinct from the others in this work. Figure 7c compares the AFM topographic profile with the cross-section |**E**| distribution. The two innermost symmetric bumps of the profile corresponding to the rim formed by the mass migration away from the area beneath the sphere due to the near-field focusing enhancement. The central rise in the dent is consistent with that observed on an azo polymer film upon irradiation with a Gaussian laser beam[59]. This is related to the stronger absorption of IA-Chol film to 488 nm light (Supplementary Fig. 11). For the topographic cross-sections of other concentric rings, the valleys between the rings correspond to the higher |**E**| region, whilst the ridges of the rings correspond to the lower |**E**| region. As shown by FEM simulation, the polarization state of the *E*-field is almost not affected around the polystyrene sphere (Supplementary Fig. 39a, b). These results indicate that the formation of the encircling relief structures around the sphere is caused by the mass transfer of IA-Chol along electric vibration direction from the higher |**E**| areas to lower |**E**| areas (Fig. 7d). This mass transfer behavior has been well observed on azo materials for the SRG formation and dent inscription under the light irradiation[12,13,55–59].

In the second stage of the pattern formation upon CPL irradiation, the rings split into hillocks with the increase in the irradiation time (Fig. 7e, f). In the process, the emerging hillocks with local hexagonal order preserve the geometric characteristics of concentric relief rings (Fig. 7g), i.e., the arrangements of hillocks are controlled by the circular relief structures formed in first 10 min upon CPL irradiation. Figure 8 compares the SEM images of the relief structures upon the CPL irradiation at 488 nm for 10 min (black and white) with the |**E**| distributions (color) obtained by FEM calculation (COMSOL Multiphysics). As identically observed in areas around one sphere (Fig. 8a), two spheres (Fig. 8b–f) and three spheres (Fig. 8g, h), the ridges of the formed relief structures situate in the regions with the relatively
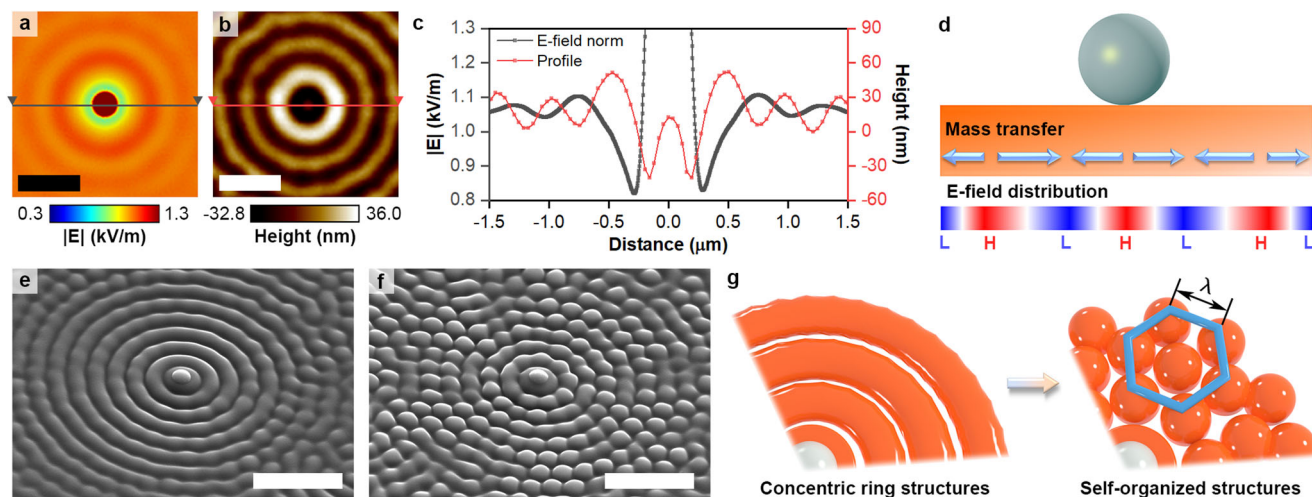
Fig. 7 The *E*-field norm distribution simulated by COMSOL Multiphysics, the topography of IA-Chol film, and the illustration of self-organized hillock pattern formation. a The *E*-field norm distribution on the film surface simulated by COMSOL Multiphysics. **b** The AFM image of the surface after being exposed to the circularly polarized light ($\lambda = 488$ nm) for 10 min. **c** The cross-section of *E*-field norm distribution and AFM profile of the film surface. **d** The illustration of the mass transfer direction. **e**, **f** Side-view SEM images of IA-Chol films with polystyrene spheres ($D = 500$ nm) on the surfaces exposed to the circularly polarized light ($\lambda = 488$ nm) for 20 min and 30 min, respectively. **g** Schematic illustration of the ring-to-hillock transition in the process, where the hexagonal local structures almost remain intact to fit in the circular arrangement. The light intensity was 300 mW cm^{-2}. The scale bars in **a**, **b** correspond to 1 μm and the scale bars in the SEM images (**e**, **f**) correspond to 2 μm.
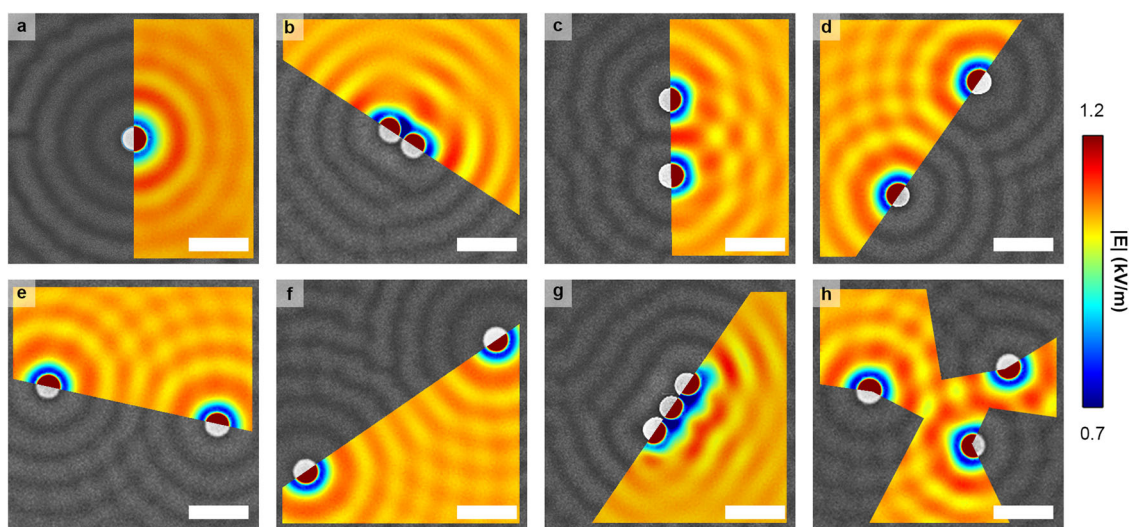

Fig. 8 Comparison of the *E*-field norm distribution (color) simulated by COMSOL Multiphysics with the top-view SEM images of the IA-Chol films (black and white) with polystyrene spheres ($D = 500$ nm) on the surfaces after being exposed to the circularly polarized light for 10 min. a Single polystyrene sphere. **b**-**f** Two polystyrene spheres. **g**, **h** Three polystyrene spheres. The light intensity and wavelength were 300 mW cm^{-2} and 488 nm. The scale bars in all the SEM images correspond to 1 μm.

low |**E**|, while the grooves of the structures correspond to the regions with relatively high |**E**|. Even though the interference patterns of the scattered lights from spheres and incident light become complicated in the areas, the structures formed in this stage still well replicate the interference patterns through the mass transfer induced by CPL irradiation. In the second stage, the average distances (d) between the two adjacent hillocks are not affected by ring-to-hillock transition, which are almost the same as those formed on surface not affected by the scattered light and approximately equal to the light wavelengths (Supplementary Table 1, 2). Therefore, the average number of hillocks in each circle (N_i) is determined by the following relationship,

$$2\pi R_i = d \times N_i \tag{1}$$

where R_i is radius of each circular array obtained from SEM

(Supplementary Fig. 40). The calculated N_i values are in good agreement with the numbers of hillocks counted from SEM images (Supplementary Fig. 41, Supplementary Table 3).

Influences of dynamic factors. As the self-organized pattern formation is not an instant process, it includes a series of dynamic and time-retarded responses of material to the light irradiation. Although the formed structures are controlled by the interference fields around the spheres, the radii of circular hillock arrays change with the irradiation time (Supplementary Table 4). It means that the surfaces around the spheres undergo a dynamic variation upon the CPL irradiation, where the partial immersion of polystyrene spheres during CPL irradiation (Supplementary Fig. 35) plays an important role in the process. To understand the

influence of sphere sinking on the light scattering behavior, the interference fields at several intermediate stages were calculated by COMSOL Multiphysics. As shown in Supplementary Figs. 42 and 43, the interference patterns around polystyrene spheres undergo a significant variation in the first 5 min and then slightly change with irradiation time. Comparing with the results given in Supplementary Table 4, it can be seen that the radii of the rings at the irradiation for 10 min are more closely related to the interference patterns of original configurations without sinking, while the radii at 20 and 30 min are obviously influenced by the varied interference field due to the partial sphere immersion. This observation can be explained by considering the Boltzmann superposition principle as follows,

$$\gamma(t) = \gamma_0 + \int_{-\infty}^{t} J(t-\tau)\frac{\partial \sigma(\tau)}{\partial \tau}d\tau \qquad (2)$$

where $\gamma(t)$ is the deformation at time t, γ_0 is the immediate elastic deformation, $J(t-\tau)$ is the creep compliance function and $\sigma(\tau)$ is the stress at all previous instants[67]. Therefore, the deformation observed at t is a result of continuously exerted stress and varied compliance in the process, in the current case, both of which are related to light irradiation. It means that the structure observed at the moment is an accumulated effect of the irradiation history. As azo chromophores can be driven by CPL to align perpendicularly to the electric vibration direction[13,16], the light absorption and trans-cis isomerization efficiency to cause mass transfer will be markedly reduced in few minutes. Therefore, the interference light field from the original configuration without sinking is more important to determine the ring sizes in the first 10 min. On the other hand, with the continuous CPL irradiation for a longer period, the interference fields related to the partially immersed polystyrene spheres play a more important role to influence the self-organized hillock arrays. Therefore, the radii of the circular arrays do not keep to the values obtained in the first stage (Supplementary Table 4), which vary with the irradiation for 20 and 30 min due to the immersion of the spheres in the films. Because of the larger scale immersion of polystyrene spheres under the irradiation with 488 nm light, the ring radius variations are observed to be more significant. The displacement of the material from the space beneath the sphere could play a role to cause the ring expansion, which is also larger for 488 nm radiation.

These radius variations bring the annular ridges to leave the areas with lower light intensity, which is necessary for the ring-to-hillock transition in the second stage. Although the circular organization is controlled by the relief patterns formed in the first stage, the local order and radii of the finally formed circular arrays are determined by the hillock formation mechanism. As the distances between the adjacent hillocks are almost equal to the wavelengths, the dynamic radius adjustment becomes necessary to accommodate the formed hillocks with the local hexagonal order. Once the hillocks start to form, the radii of the circular arrays spontaneously adjust to compromise with the hexagonal arrangement. Therefore, there are some irregular variations of the radii (R_i) appearing in the second stage of the pattern formation. However, as the distance d in Eq.(1) is equal to the wavelength and N_i is weakly correlated with the wavelength, R_i is roughly proportional to the wavelength of CPL after the irradiation for 30 min (Supplementary Table 3).

Methods

Materials. Isosorbide, 4-nitrobenzoyl chloride, (N-ethyl-N-hydroxyethyl)aniline, and cholesteryl chloroformate were purchased from Alfa Aesar Co. The concentrated sulfuric acid, glacial acetic acid, dichloromethane (DCM) and N,N-dimethylformamide (DMF) were purchased from commercial sources as analytical pure products. The deionized water (resistivity >18.0 MΩ cm) was obtained from a

Milli-Q water purification system. The reagents and solvents not mentioned above were commercial products and used as received without further purification. The polystyrene microspheres with average diameters of 250, 500, and 1000 nm were purchased from Wuxi rigor bio-tech Co. Ltd, which had refractive index of 1.6 and diameter deviations in a range of ±5%. The glass slides (ultra-clear glass) were a commercial product (Citotest Scientific Co., Ltd.) with refractive index of 1.5. The azo molecular glass (IA-Chol) was synthesized according to the method reported by us previously[60], which is also presented in detail in the Supplementary.

Preparation of IA-Chol thin film with polystyrene particles on the surface. A homogeneous solution was prepared by dissolving IA-Chol in DMF with a typical concentration of 10 wt%, which was filtered through 0.45 μm membrane before use. Thin films of IA-Chol with a smooth surface were prepared by spin-coating the DMF solution (10 wt%) on the clean glass slides (ultra-clear glass, Citotest Scientific Co., Ltd.) at a speed of 1200 rpm for 30 s, and then dried at 50 °C under vacuum for 48 h before use. The thicknesses of the films were measured by AFM to be in a range from 300 to 400 nm. The commercially obtained suspensions of polystyrene microspheres in deionized water were properly diluted to ensure the spreading distribution of the spheres on the film surfaces. Drops of the suspensions were then added by a micro pipette onto the IA-Chol thin films, which were dried at room temperature for 24 h before use.

Light irradiation setup. A semiconductor laser (488 nm, Genesis CX 488–2000 SLM, Coherent Corporation) and a diode-pumped frequency doubled solid-state laser (532 nm, MGL-F-532, Changchun New Industries Optoelectronics Tech. Co., Ltd) were used as the light source, respectively. The laser beam was expanded with a spatial filter and collimated by a convex lens to obtain a homogenous beam with a diameter of 20 mm. An aperture with an adjustable diameter was used to control the area of irradiation. A polarizer was placed in the light path to ensure high linear polarization. A quarter-wave ($\lambda/4$) plate, where its fast axe was oriented by 45° to the vibration direction of the linearly polarized incoming beam, was applied to achieve circular polarization. Most of the experiments were performed by setting a broadband dielectric mirror (450–700 nm, GCC-101102, Daheng New Epoch Technology, Inc.) with an angle of 45° to let the reflected beam travel perpendicularly to the optical bench. The sample was placed horizontally on the surface of the optical breadboard to ensure that the polystyrene spheres did not fall off during the irradiation process. For the case to view the surface morphology beneath the spheres, the beam propagated parallel to the optical bench and struck the sample placed vertically on the breadboard, for which some polystyrene spheres fell off from the surface during the irradiation. The intensity of CPL and LPL was 300 mW cm^{-2}, which was also reduced to 150 mW cm^{-2} for investigating the light intensity effect, and the irradiation was performed for a required time period under ambient conditions.

Model and calculation. All the results of the optical simulation were obtained by COMSOL Multiphysics (version 5.6, COMSOL, Inc.) with the wave optics module. For the electromagnetic wave with the angular frequency (ω) and the speed in vacuum (c_0), Maxwell's equation in three dimensions is given

$$\nabla \times \left(\mu_r^{-1}\nabla \times \mathbf{E}\right) - \frac{\omega^2}{c_0^2}\left(\varepsilon_r - \frac{i\sigma}{\omega\varepsilon_0}\right)\mathbf{E} = 0 \qquad (3)$$

where μ_r is the relative permeability, ε_r is the relative permittivity, and σ is the electrical conductivity of the materials. The above equation is solved for the electric field $\mathbf{E}$ throughout the modeling domains by FEM. The continuous domain of the light field is replaced by a finite number of subdomains in which the unknown function is represented by simple interpolation functions with unknown coefficients[68]. Therefore, the problem to solve Maxwell's equation with boundary values is converted into a problem with a finite number of degrees, approximated by a finite number of coefficients to be optimized. In the calculation, the entire modeling domain is divided into the air layer, IA-Chol thin film layer, and glass layer (Supplementary Fig. 44). The incident light port setting for optical simulations is shown in Supplementary Fig. 45. The complex refractive indices of the IA-Chol films were obtained by ellipsometry and used for the calculation. The complex refractive indices had the real part (n) of 1.84, and the imaginary part (κ) of 0.46 at 488 nm, n of 1.99 and κ of 0.12 at 532 nm (Supplementary Fig. 46). The refractive index of 1.6 is adopted for polystyrene spheres and the refractive index of glass is set to be 1.5 in the calculation.

Characterization. The ^{1}H NMR and ^{13}C NMR spectra were obtained on JEOL JNM-ECA 600 and JNM-ECS 400 spectrometers with tetramethylsilane as the internal standard in a solution of CDCl$_3$ or DMSO-d_6 at 30 °C. The FT-IR spectra were collected on a Nicolet 560-IR spectrometer, where the powder samples were ground, mixed with KBr, and then pressed into thin IR-transparent disks. High-resolution mass spectra were recorded on a XEVO G2 QTOF mass spectrometer. The surface patterns were observed by an SEM instrument from Zeiss Corporation (Zeiss Merlin). A high vacuum (~4 × 10^{-6} mbar) condition was adopted, where the applied voltage and current were l5 kV and 100 pA, respectively. The surface topography and profile of the samples were probed using an AFM from the Bruker Corporation (Dimension ICON-PT) in tapping mode. The optical images of

polystyrene particles were captured by a Nikon LV 100 POL microscope equipped with a Nikon DS-fi2 CCD camera. The complex refractive indices of the IA-Chol were measured by the elliptical polarization spectrometer (Sentech Instruments SE850).

Data availability

Code availability

References

1. Jacobs, H. O., Tao, A. R., Schwartz, A., Gracias, D. H. & Whitesides, G. M. Fabrication of a cylindrical display by patterned assembly. *Science* **296**, 323–325 (2002).
2. van Hameren, R. et al. Macroscopic hierarchical surface patterning of porphyrin trimers via self-assembly and dewetting. *Science* **314**, 1433–1436 (2006).
3. Briseno, A. L. et al. Patterning organic single-crystal transistor arrays. *Nature* **444**, 913–917 (2006).
4. Liao, W. S. et al. Subtractive patterning via chemical lift-off lithography. *Science* **337**, 1517–1521 (2012).
5. Lin, D., Fan, P., Hasman, E. & Brongersma, M. L. Dielectric gradient metasurface optical elements. *Nature* **345**, 298–302 (2014).
6. Lassaline, N. et al. Optical Fourier surfaces. *Nature* **582**, 506–509 (2020).
7. Ito, T. & Okazaki, S. Pushing the limits of lithography. *Nature* **406**, 1027–1031 (2000).
8. Carlson, A., Bowen, A. M., Huang, Y. G., Nuzzo, R. G. & Rogers, J. A. Transfer printing techniques for materials assembly and micro/nanodevice fabrication. *Adv. Mater.* **24**, 5284–5318 (2012).
9. Khorasaninejad, M. & Capasso, F. Metalenses: versatile multifunctional photonic components. *Science* **358**, eaam8100 (2017).
10. Qiao, W. et al. Toward scalable flexible nanomanufacturing for photonic structures and devices. *Adv. Mater.* **28**, 10353–10380 (2016).
11. Hölz, K., Schaudy, E., Lietard, J. & Somoza, M. M. Multi-level patterning nucleic acid photolithography. *Nat. Commun.* **10**, 3805 (2019).
12. Viswanathan, N. K. et al. Surface relief structures on azo polymer films. *J. Mater. Chem.* **9**, 1941–1955 (1999).
13. Natansohn, A. & Rochon, P. Photoinduced motions in azo-containing polymers. *Chem. Rev.* **102**, 4139–4176 (2002).
14. Ubukata, T., Hara, M., Ichimura, K. & Seki, T. Phototactic mass transport in polymer films for micropatterning and alignment of functional materials. *Adv. Mater.* **16**, 220–223 (2004).
15. Yu, H. F. et al. Enhancement of surface-relief gratings recorded on amphiphilic liquid-crystalline diblock copolymer by nanoscale phase separation. *Adv. Mater.* **17**, 2184–2188 (2005).
16. Shirota, Y. Photo- and electroactive amorphous molecular materials—molecular design, syntheses, reactions, properties, and applications. *J. Mater. Chem.* **15**, 75–93 (2005).
17. Lee, S., Kang, H. S. & Park, J.-K. Directional photofluidization lithography: micro/nanostructural evolution by photofluidic motions of azobenzene materials. *Adv. Mater.* **24**, 2069–2103 (2012).
18. Priimagi, A. & Shevchenko, A. Azopolymer-based micro- and nanopatterning for photonic applications. *J. Polym. Sci., Part B: Polym. Phys.* **52**, 163–182 (2014).
19. Wang, X. G. *Azo Polymers: Synthesis, Functions and Applications* Ch. 5 (Springer-Verlag, Berlin, 2017).
20. Oscurato, S. L., Salvatore, M., Maddalena, P. & Ambrosio, A. From nanoscopic to macroscopic photo-driven motion in azobenzene-containing materials. *Nanophotonics* **7**, 1387–1422 (2018).
21. Dattler, D. et al. Design of collective motions from synthetic molecular switches, rotors, and motors. *Chem. Rev.* **120**, 310–433 (2020).
22. Rochon, P., Batalla, E. & Natansohn, A. Optically induced surface gratings on azoaromatic polymer films. *Appl. Phys. Lett.* **66**, 136–138 (1995).
23. Kim, D. Y., Tripathy, S. K., Li, L. & Kumar, J. Laser-induced holographic surface relief gratings on nonlinear optical polymer films. *Appl. Phys. Lett.* **66**, 1166–1168 (1995).
24. Hubert, C. et al. Near-field photochemical imaging of noble metal nanostructures. *Nano Lett.* **5**, 615–619 (2005).
25. Haggui, M. et al. Spatial confinement of electromagnetic hot and cold spots in gold nanocubes. *ACS Nano* **6**, 1299–1307 (2012).
26. Kim, M. et al. Photofluidic near-field mapping of electric-field resonance in plasmonic metasurface assembled with gold nanoparticles. *J. Phys. Chem. Lett.* **8**, 3745–3751 (2017).
27. Ambrosio, A., Marrucci, L., Borbone, F., Roviello, A. & Maddalena, P. Light-induced spiral mass transport in azo-polymer films under vortex-beam illumination. *Nat. Commun.* **3**, 989 (2012).
28. Hubert, C., Fiorini-Debuisschert, C., Maurin, I., Nunzi, J. M. & Raimond, P. Spontaneous patterning of hexagonal structures in an azo-polymer using light-controlled mass transport. *Adv. Mater.* **14**, 729–732 (2002).
29. Hubert, C., Fiorini-Debuisschert, C., Rocha, L., Raimond, P. & Nunzi, J.-M. Spontaneous photoinduced patterning of azo-dye polymer films: the facts. *J. Opt. Soc. Am. B: Opt. Phys.* **24**, 1839–1846 (2007).
30. Yin, J. J., Ye, G. & Wang, X. G. Self-structured surface patterns on molecular azo glass films induced by laser light irradiation. *Langmuir* **26**, 6755–6761 (2010).
31. Wang, X. L., Yin, J. J. & Wang, X. G. Photoinduced self-structured surface pattern on a molecular azo glass film: structure–property relationship and wavelength correlation. *Langmuir* **27**, 12666–12676 (2011).
32. Wang, X. L., Yin, J. J. & Wang, X. G. Self-structured surface patterns on epoxy-based azo polymer films induced by laser light irradiation. *Macromolecules* **44**, 6856–6867 (2011).
33. Nakano, H., Takahashi, T., Kadota, T. & Shirota, Y. Formation of a surface relief grating using a novel azobenzene-based photochromic amorphous molecular material. *Adv. Mater.* **14**, 1157–1160 (2002).
34. Ishow, E., Bellaïche, C., Bouteiller, L., Nakatani, K. & Delaire, J. A. Versatile synthesis of small NLO-active molecules forming amorphous materials with spontaneous second-order NLO response. *J. Am. Chem. Soc.* **125**, 15744–15745 (2003).
35. Kim, M. J., Seo, E. M., Vak, D. J. & Kim, D. Y. Photodynamic properties of azobenzene molecular films with triphenylamines. *Chem. Mater.* **15**, 4021–4027 (2003).
36. Guo, M. C., Xu, Z. D. & Wang, X. G. Photofabrication of two-dimensional quasi-crystal patterns on UV-curable molecular azo glass films. *Langmuir* **24**, 2740–2745 (2008).
37. Walker, R., Audorff, H., Kador, L. & Schmidt, H. W. Synthesis and structure-property relations of a series of photochromic molecular glasses for controlled and efficient formation of surface relief nanostructures. *Adv. Funct. Mater.* **19**, 2630 (2009).
38. Luk'yanchuk, B. S., Paniagua-Domínguez, R., Minin, I., Minin, O. & Wang, Z. Refractive index less than two: photonic nanojets yesterday, today and tomorrow. *Opt. Mater. Express.* **7**, 1820–1847 (2017).
39. Zhang, X. A., Chen, I. T. & Chang, C. H. Recent progress in near-field nanolithography using light interactions with colloidal particles: from nanospheres to three-dimensional nanostructures. *Nanotechnology* **30**, 352002 (2019).
40. Chen, L., Zhou, Y., Li, Y. & Hong, M. Microsphere enhanced optical imaging and patterning: from physics to applications. *Appl. Phys. Rev.* **6**, 021304 (2019).
41. Born, M. & Wolf, E. *Principles of Optics: Electromagnetic Theory of Propagation, Interference and Diffraction of Light* Ch. 13 (Cambridge University Press, Cambridge England, 1999).
42. Luk'yanchuk, B. S., Zheng, Y. W. & Lu, Y. F. Laser cleaning of solid surface: optical resonance and near-field effects. *Proc. SPIE* **4065**, 576–587 (2000).
43. Wang, Z. B., Luk'yanchuk, B. S., Hong, M. H., Lin, Y. & Chong, T. C. Energy flow around a small particle investigated by classical Mie theory. *Phys. Rev. B* **70**, 035418 (2004).
44. Chen, Z. G., Taflove, A. & Backman, V. Photonic nanojet enhancement of backscattering of light by nanoparticles: a potential novel visible-light ultramicroscopy technique. *Opt. Express* **12**, 1214–1220 (2004).
45. Li, X., Chen, Z. G., Taflove, A. & Backman, V. Optical analysis of nanoparticles via enhanced backscattering facilitated by 3-D photonic nanojets. *Opt. Express* **13**, 526–533 (2005).
46. Lecler, S., Takakura, Y. & Meyrueis, P. Properties of a three-dimensional photonic jet. *Opt. Lett.* **30**, 2641–2643 (2005).
47. Münzer, H. J. et al. Local field enhancement effects for nanostructuring of surfaces. *J. Microsc.* **202**, 129–135 (2001).
48. Zhou, Y. et al. Direct femtosecond laser nanopatterning of glass substrate by particle-assisted near-field enhancement. *Appl. Phys. Lett.* **88**, 023110 (2006).
49. Piglmayer, K., Denk, R. & Bäuerle, D. Laser-induced surface patterning by means of microspheres. *Appl. Phys. Lett.* **80**, 4693 (2002).
50. Huang, S. M. et al. Pulsed laser-assisted surface structuring with optical near-field enhanced effects. *J. Appl. Phys.* **92**, 2495–2500 (2002).
51. McLeod, E. & Arnold, C. B. Subwavelength direct-write nanopatterning using optically trapped microspheres. *Nat. Nanotechnol.* **3**, 413–417 (2008).
52. Zhang, X. A., Elek, J. & Chang, C. H. Three-dimensional nanolithography using light scattering from colloidal particles. *ACS Nano* **7**, 6212–6218 (2013).

53. Zhang, X. A., Dai, B., Xu, Z. & Chang, C. H. Sculpting asymmetric, hollow-core, three-dimensional nanostructures using colloidal particles. *Small* **11**, 1285–1292 (2015).

54. Kühler, P. et al. Imprinting the optical near field of microstructures with nanometer resolution. *Small* **16**, 1825–1829 (2009).

55. Hasegawa, M., Ikawa, T., Tsuchimori, M., Watanabe, O. & Kawata, Y. Topographical nanostructure patterning on the surface of a thin film of polyurethane containing azobenzene moiety using the optical near field around polystyrene spheres. *Macromolecules* **34**, 7471–7476 (2001).

56. Keum, C. D., Ikawa, T., Tsuchimori, M. & Watanabe, O. Photodeformation behavior of photodynamic polymers bearing azobenzene moieties in their main and/or side chain. *Macromolecules* **36**, 4916–4923 (2003).

57. Ikawa, T. et al. Azobenzene polymer surface deformation due to the gradient force of the optical near field of monodispersed polystyrene spheres. *Phys. Rev. B* **64**, 195408 (2001).

58. Kumar, J. et al. Gradient force: The mechanism for surface relief grating formation in azobenzene functionalized polymers. *Appl. Phys. Lett.* **72**, 2096–2098 (1998).

59. Bian, S. et al. Photoinduced surface deformations on azobenzene polymer films. *J. Appl. Phys.* **86**, 4498–4508 (1999).

60. Hsu, C. E., Du, Y. & Wang, X. G. Janus and strawberry-like particles from azo molecular glass and polydimethylsiloxane oligomer. *Langmuir* **33**, 10645–10654 (2017).

61. Wang, Z. N., Huang, H., Hsu, C. E. & Wang, X. G. Azo molecular glass patterning from chiral submicron pillar array to self-organized topographic transition via irradiation with circularly polarized light. *Adv. Opt. Mater.* **9**, 2100922 (2021).

62. Wang, Z. N., Huang, H., Hsu, C. E. & Wang, X. G. Laser-induced transitions of azo molecular glass pillar arrays: A new way to fabricate periodic complex surface patterns upon linearly polarized radiation. *Adv. Opt. Mater.* **10**, 2102795 (2022).

63. Israelachvili, J. N. *Intermolecular and Surface Forces* Ch. 10 (Academic Press, London, 1991).

64. Zheng, Y. W., Luk'yanchuk, B. S., Lu, Y. F., Song, W. D. & Mai, Z. H. Dry laser cleaning of particles from solid substrates: experiments and theory. *J. Appl. Phys.* **90**, 2135–2142 (2001).

65. Kim, M. J. et al. Control of photodynamic motions of azobenzene-derivative polymers by laser excitation wavelength. *Macromol. Chem. Phys.* **208**, 1753–1763 (2007).

66. Wang, X. L., Yin, J. J. & Wang, X. G. Epoxy-based polymers functionalized with bisazo chromophores: Synthesis, characterization and photoresponsive behavior. *Polymer* **52**, 3344–3356 (2011).

67. Ward, I. M. *Mechanical Properties of Solid Polymers* (second edition) Ch. 5 (John Wiley & Sons Inc., New York, 1983).

68. Jin, J. M. *The Finite Element Method in Elcctromagnetics* (third edition) Ch. 2 (John Wiley & Sons Inc., New Jersey, 2014).

Author contributions
Z.W. and X.W. conceived the idea of this work. Z.W. performed the experiments, measurements and data analysis. Z.W. and H.H. performed the simulation calculations. X.W. supervised the whole work. Z.W. and X.W. analyzed the results and wrote the manuscript.

Competing interests
The authors declare no competing interests.

Additional information
Supplementary information The online version contains supplementary material available at https://doi.org/10.1038/s43246-023-00361-8.

Correspondence and requests for materials should be addressed to Xiaogong Wang.

Peer review information *Communications Materials* thanks Eléna Ishow, Sohrab Ahmadi-Kandjani, and the other, anonymous, reviewer(s) for their contribution to the peer review of this work. Primary Handling Editors: Jet-Sing Lee and Aldo Isidori.

Reprints and permission information is available at http://www.nature.com/reprints

Publisher's note Springer Nature remains neutral with regard to jurisdictional claims in published maps and institutional affiliations.